Research Article

NaOH-Activated Carbon from *Gnetum gnemon* L. Shell Waste for Methylene Blue Adsorption from Aqueous Solutions

Lelifajri*, Amiera Hafizhah and Khairi
Department of Chemistry, Faculty of Mathematics and Natural Sciences, Universitas Syiah Kuala, Banda Aceh, Indonesia

Andriy Anta Kacaribu
Doctoral Program of Agricultural Science, Postgraduate School, Universitas Syiah Kuala, Banda Aceh, Indonesia

* Corresponding author. E-mail: lelifajri@usk.ac.id
DOI: 10.14416/j.asep.2026.02.010
Received: 2 October 2025; Revised: 24 November 2025; Accepted: 23 December 2025; Published online: 24 Febuary 2026

Abstract
Synthetic dyes, such as methylene blue (MB), are widely used in textile and related industries, and their discharge into aquatic environments poses severe environmental and health risks due to their toxicity, persistence, and poor biodegradability. This study reports the preparation of activated carbon derived from melinjo (*Gnetum gnemon* L.) shell waste (MSAC) through carbonization at 300 °C for 1 h, followed by chemical activation using NaOH solutions (1–4 M) for 24 h. NaOH activation of G. *gnemon* shell carbon is introduced for the first time to enhance its surface characteristics and adsorption performance. Structural and surface modifications before and after activation were characterized by FTIR and SEM-EDX analyses. Batch adsorption experiments were performed to evaluate the effects of contact time, initial pH of MB, and dye concentration on MB removal. NaOH activation significantly improved the surface functionality and porosity of MSAC, resulting in a maximum adsorption capacity (Q_{max}) of 148.214 mg/g at pH 7.0 and an initial concentration of 200 ppm within 35 min. The adsorption process followed the Langmuir isotherm (R^2 = 0.963) and pseudo-second-order kinetics, indicating monolayer chemisorption on a homogeneous surface. These findings demonstrate that NaOH activation effectively enhances the adsorption performance of *G. gnemon* shell waste–based carbon, making it a low-cost, sustainable adsorbent for the treatment of dye-laden wastewater.

Keywords: Adsorption, Melinjo shell waste activated carbon (MSAC), Methylene blue, NaOH activation, Wastewater treatment

1 Introduction

The rapid advancement of technology and industrial growth has led to an increasing problem of wastewater generation [1]. Among various industrial effluents, textile wastewater is one of the most problematic because of its high content of synthetic dyes used during dyeing processes [2]. The textile sector significantly contributes to the national economy as a source of foreign exchange; however, it also creates severe environmental challenges due to the discharge of dye–containing wastewater [3]. Textile dyes are generally classified into anionic, cationic, and non–ionic types, with methylene blue (MB) being one of the most widely used cationic dyes [4], [5]. MB is toxic, non–biodegradable, and water–soluble, making it a persistent pollutant that endangers aquatic ecosystems and human health [4], [6]. Recent studies reaffirm that MB–containing effluents are among the most difficult to manage due to their chemical stability and environmental persistence [7], [8].

To address dye contamination, various treatment methods have been developed, including coagulation/flocculation [9], advanced oxidation, membrane filtration [10], [11], ozonation [12], liquid–liquid extraction [13], and adsorption [14]. Among

these, adsorption stands out as the most efficient and economical method owing to its simplicity, flexibility, and high removal efficiency [15]. Several adsorbent materials, such as modified cellulose [16], polylactic acid (PLA) [17], [18], chitosan [19], and graphene oxide [20], have been explored. Despite their excellent adsorption properties, these materials often require costly chemicals, multi-step synthesis, and complex processing, limiting their large-scale application—particularly in developing countries like Indonesia [20].

Consequently, activated carbon (AC) remains the most widely adopted adsorbent due to its high surface area, tunable pore structure, and excellent adsorption capacity [21], [22]. It is typically prepared from carbon–rich precursors, particularly agricultural residues, through carbonization and activation processes [23]. Activation can be achieved either physically—via high-temperature treatment with oxidizing gases (e.g., steam, CO_2) [24]—or chemically using activating agents such as KOH or NaOH [5], [25]. NaOH was selected in this study due to it effectively promotes the development of micro– and mesopores through strong alkaline etching, facilitating the removal of tars and inorganic impurities, and enhancing oxygen–containing surface functionalities. Compared with other chemical activators such as KOH, NaOH offers high activation efficiency at lower temperatures and at a lower cost, making it an advantageous choice for producing highly porous activated carbon. Recent findings also indicate that NaOH activation produces smoother and more hydroxylated surfaces with improved chemical reactivity and uniformity, whereas KOH tends to generate denser morphologies with greater microporosity and thermal stability [26]. Various agricultural wastes, including empty fruit bunch (EFB) [27], bamboo [28], seaweed [5], and peanut shells [29], have been successfully transformed into AC for dye removal.

Agricultural waste offers a sustainable and low–cost opportunity for developing high–performance adsorbents while supporting circular economy principles. *Gnetum gnemon* shell waste, locally known as "Melinjo," is an abundant lignocellulosic biomass composed primarily of cellulose, hemicellulose, and lignin. Previous studies have demonstrated its potential as an efficient precursor for MB adsorption. Lelifajri *et. al.,* produced thermally activated G. *gnemon* shells waste at 250–400 °C and obtained a maximum MB adsorption capacity (Q_{max}) of 35.58 mg/g under Langmuir isotherm conditions [30]. Our previous work further enhanced its performance through chemical activation using NaCl after thermal treatment, achieving a Q_{max} of 62.5 mg/g [31]. These studies demonstrate that progressive modification—transitioning from physical to chemical activation—can substantially improve the adsorption capability of G. gnemon–derived activated carbon.

However, despite these advances, no studies have yet examined the use of alkaline chemical activation (NaOH) for *G. gnemon* shell waste–based activated carbon. Specifically, the effect of NaOH concentration on adsorption performance remains unexplored and comprehensive characterized. This represents a significant gap in the current understanding of how chemical activation conditions influence the structural and functional characteristics of AC derived from this biomass. Recent work by Setiawan *et. al.,* [32] has shown that varying NaOH and KOH concentrations during activation can significantly modify surface area and chemical functionality in carbon–based materials, reinforcing the importance of optimizing alkali treatment parameters for performance enhancement.

Therefore, this study aims to develop activated carbon from *G. gnemon* shell waste via chemical activation using NaOH at various concentrations and to evaluate its adsorption performance for methylene blue removal from aqueous solutions. This research seeks to fill the identified knowledge gap and contribute to a sustainable solution for dye–contaminated wastewater. Moreover, it supports SDG 6 (Clean Water and Sanitation) by providing a low–cost, effective adsorbent, and SDG 12 (Responsible Consumption and Production) by valorizing agricultural waste within a circular economy framework [33], [34].

2 Materials and Methods

2.1 *Materials*

The materials used in this study included methylene blue solution ($C_{16}H_{18}N_3SCl$), sodium hydroxide (NaOH), and hydrochloric acid (HCl), all of analytical grade and purchased from Merck (Selangor, Malaysia). Distilled water, filter paper, and melinjo (*G. gnemon* L.) shell waste collected from emping cracker production in Kembang Tanjong, Pidie District, Indonesia, were used as raw materials.

2.2 *Activated carbon preparations*

The preparation of activated carbon was carried out following the procedure reported previously [31] with

slight modifications. Melinjo shell waste was separated from impurities such as gravel, sand, and wood. The sample was washed thoroughly with distilled water to remove adhering soil and other contaminants, and then dried in an oven at 105 °C for 1 h. The dried sample was carbonized using a tubular furnace (Carbolite Gero STF 15/450, UK) under a nitrogen atmosphere to prevent oxidation of the sample during heating. About 20 g of the dried biomass was placed in a ceramic crucible and heated from room temperature to 300 °C at a heating rate of 10 °C/min, followed by holding at this temperature for 1 h. The resulting carbon was ground using a mortar and sieved through a 100–mesh sieve. The obtained carbon was subsequently activated by soaking in NaOH solution (solid–to–liquid ratio 1:1) with concentrations of 1, 2, 3, and 4 M, as illustrated in Figure 1. This figure is presented to visually demonstrate the actual activation process and concentration variations during NaOH treatment. The samples shown were still in the soaking stage and, therefore, appear wet. The mixtures were kept at 50 °C under continuous stirring at 100 rpm for 24 h. After activation, the carbon was filtered and washed with distilled water until a neutral pH was reached, followed by drying in an oven at 105 °C until constant weight, melinjo shell waste activated carbon (MSAC) was obtained. Yield, moisture content, and ash content of MSAC obtained at optimal conditions were determined.

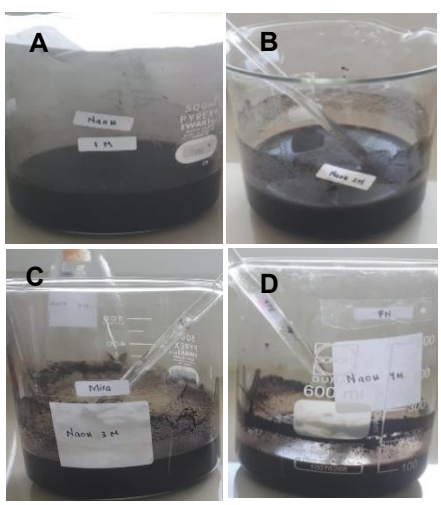

Figure 1: Activation of melinjo shell waste–derived carbon using various concentrations of NaOH: (A) 1 M; (B) 2 M; (C) 3 M; and (D) 4 M.

2.3 *Adsorption study*

The adsorption experiments were conducted under various operating conditions and described as follows. A stock solution of methylene blue (MB, 1000 ppm) was prepared by dissolving 1 g of MB in 1000 mL of distilled water. The maximum absorption wavelength (λ_{max}) was determined using a 3 ppm MB solution. λ_{max} obtained in the present study is presented in Figure 2A (622 nm). A calibration curve was obtained by preparing MB solutions of 1, 2, 3, 4, 5, 6, and 7 ppm, and the absorbance was measured using a UV–Vis spectrophotometer (Shimadzu UV-Mini 1240). The calibration curve was plotted with absorbance versus concentration, as shown in Figure 2B. The MB standard solutions were prepared in distilled water at natural pH (6.8–7.0) to maintain consistency with the adsorption experiment conditions.

To determine the optimal activation condition for MSW–derived carbon, 0.1 g of activated carbon from different treatments was added to 15 mL of a 100 ppm MB solution and shaken at 250 rpm for 10 min at room temperature (25–27 °C). The filtrate was analyzed by UV–Vis spectrophotometry at λmax. The removal efficiency of MB (%R), the adsorption capacity at equilibrium (Q_e, mg/g), and adsorption capacity at t time (Q_t) were calculated using Eqs. (1)–(3):

$$\%R = \frac{C_0 - C_e}{C_0} \times 100 \quad (1)$$

$$Q_e = \frac{C_0 - C_e}{m} \times V \quad (2)$$

$$Q_t = \frac{C_0 - C_t}{m} \times V \quad (3)$$

where %R, Q_e, and Q_t represent the percentage removal, the amount of MB adsorbed at equilibrium and MB adsorbed at interval time, respectively; C_0, C_e, and C_t are the initial, equilibrium concentrations, and t time (ppm); V is the solution volume (L); and m is the adsorbent mass (g).

The effects of contact time and initial pH of the MB solution in adsorption by MSAC were also investigated. Contact time was varied from 5 to 50 min, while the initial pH of the MB solution was adjusted to 2, 4, 6, 7, 8, 10, and 12 (using 0.1 M HCl or 0.1 M NaOH solutions). Additional experiments were performed at different initial MB concentrations (150, 200, and 250 ppm) to evaluate equilibrium adsorption isotherms. The adsorption data were fitted to the non–linear Langmuir, Freundlich, Sips, and Temkin models

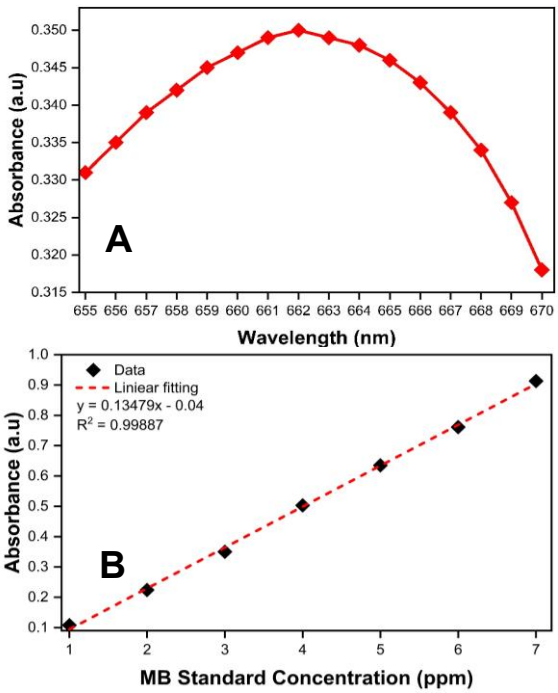

Figure 2: (A) Determination of λ_{max} of MB using UV–Vis spectrophotometer; (B) standard calibration curve of MB.

2.4 *Characterizations*

Melinjo shell waste powder (MSP) and melinjo shell waste activated carbon (MSAC) were characterized to analyze their structural and morphological properties. Fourier transform infrared spectroscopy (FTIR, FT–IR 630, Agilent Technologies) was employed to identify the functional groups present in the samples. Surface morphology and elemental composition were examined using scanning electron microscopy coupled with energy–dispersive X–ray spectroscopy (SEM–EDX, Thermo Scientific).

3 Result and Discussions

3.1 *Optimum condition of activation*

The melinjo shell waste used in this study served as a biomass source for activated carbon production. The raw melinjo shell waste exhibited a brownish color (Figure 3(A)), but after carbonization, it turned black, indicating the formation of carbon (Figure 3(B)). The carbon was formed as a result of the thermal degradation of organic components such as cellulose, hemicellulose, and lignin during the carbonization process. The obtained carbon was then ground and subsequently activated with NaOH (Figure 3(C)).

Figure 3: Visual photograph of: (A) melinjo shell waste; (B) melinjo shell after carbonization; and (C) melinjo shell waste activated carbon (MSAC) at optimum condition (2M).

In the present study, four different NaOH concentrations were prepared (as described in section 2.2) to evaluate the characteristics and adsorption performance of MSAC and to determine the optimum condition for MB removal from water. Chemical activation with NaOH aims to enlarge pore diameter and open the blocked pores of carbon by degrading residual tars and inorganic impurities [35]. This process significantly enhanced the adsorption performance of the activated carbon [36].

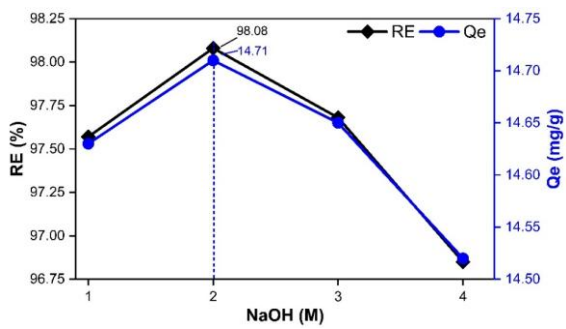

Figure 4: Optimum condition of MSC activation using NaOH. Experimental condition: MB initial concentration 100 ppm, volume 0.015 L, adsorbent dosage 0.1 g, neutral pH, contact time 60 min, at 25 °C.

The highest adsorption performance in the present study was obtained for MSAC activated with 2 M NaOH, yielding a removal efficiency (%R) of 98.08% and an adsorption capacity (Q_e) of 14.71 mg/g (Figure 4). A decrease in both %R and Q_e was observed for MSAC activated with NaOH concentrations higher than 2 M. Studies have shown that this decline can be attributed to the saturation of the carbon surface, a condition where the available active sites are fully occupied and further activation may cause partial collapse or blockage of pores affected by excessive alkaline activation [25], [37], [38]. Therefore, MSAC activated with 2 M NaOH was

selected for further analysis. The yield of MSAC under the optimal condition was 48.95%. The relatively low yield (48.95%) can be attributed to mass loss during both the carbonization and NaOH activation steps. Significant volatilization of organic matter occurs during carbonization, while the subsequent activation process promotes pore development through alkaline etching, leading to further reduction in solid yield. This trade–off between yield and surface development is a common characteristic of chemically activated carbons. In addition, the moisture content and ash content of the MSAC were 7.96% and 5.22%, respectively. These values are below the maximum limits recommended by the Indonesian National Standard (SNI) for activated carbon (15% for moisture content and 10% for ash content) [39].

3.2 *Characterizations*

3.2.1 SEM-EDX analysis

SEM–EDX analysis was performed to examine the surface morphology and elemental composition of the materials. The SEM images of the adsorbent before and after activation are presented in Figure 5. The surface morphology of melinjo shell waste carbon (MSC) before activation (Figure 5(A)) appeared rough, containing impurities, and exhibited only a few pores. The SEM image of carbonized melinjo shell waste carbon before activation (Figure 5(A)) clearly shows the formation of initial pores and surface roughness, which are likely produced during the carbonization of biomass components such as lignin, cellulose, and hemicellulose as they thermally decompose into a carbon-rich structure. In contrast, the SEM image of MSAC prepared under optimal activation conditions (Figure 5(C)) revealed a cleaner surface with a more uniform texture and significantly larger pore development. This improvement can be attributed to the effect of alkaline activation, which further enhances pore opening and surface development in activated carbon [40].

The morphological transition from a compact and impurity–rich surface to a highly porous structure clearly demonstrates the efficiency of NaOH activation in generating more accessible adsorption sites. Although Brunauer–Emmett–Teller (BET) surface area analysis was not performed, the observed evolution of pore texture in SEM images strongly supports the formation of a more developed porous network that contributes to the increased adsorption capacity of MSAC.

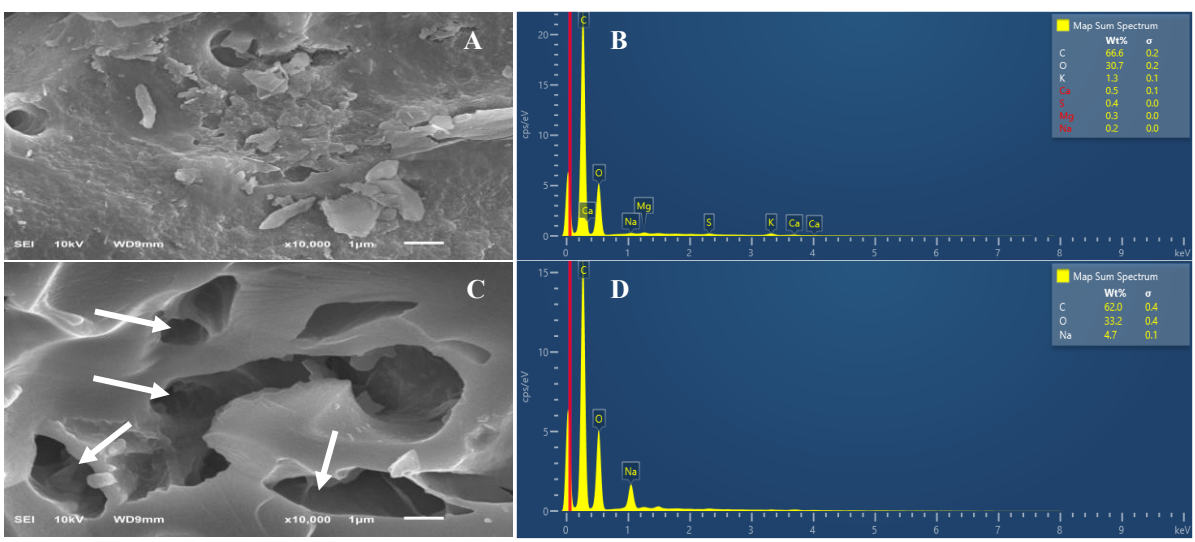

Figure 5: SEM–EDX of: (A–B) carbonized melinjo shell waste carbon before activation (MSC) and (C–D) melinjo shell waste activated carbon after NaOH treatment (MSAC) (activated under optimal conditions).

The EDX analysis of the adsorbents before and after activation revealed different elemental compositions, as shown in Figure 5(B) and (D). The spectrum of MSC indicated the presence of carbon (66.6%), oxygen (30.7%), sodium (0.2%), calcium (0.5%), magnesium (0.3%), sulfur (0.4%), and potassium (1.3%). These elements, particularly the inorganic impurities such as Ca, Mg, S, and K, are

suspected to block the pores of melinjo shell waste carbon. Such a blocking effect is consistent with reports that residual metal or inorganic salts within carbon matrices may inhibit pore formation or accessibility in activated carbons (e.g., high K, Ca content altering pore topology) [41], [42]. In contrast, the EDX spectrum of MSAC showed carbon (62.0%), oxygen (33.0%), and sodium (4.7%). This result suggests that most inorganic impurities were effectively removed after chemical activation with NaOH, leading to cleaner and more open pores [43].

Interestingly, the sodium content increased from 0.2% in MSC to 4.7% in MSAC. This increase may be attributed to the incomplete removal of residual NaOH during the washing process or the incorporation of sodium ions into oxygen–containing functional groups on the carbon surface during thermal treatment. Such interactions are likely ionic or electrostatic in nature, where Na^+ binds with negatively charged sites such as $–COO^-$ or –OH groups, and in some cases may form sodium oxide or carbonate species (Na–O–C, Na_2CO_3). The presence of sodium, therefore, not only indicates the effectiveness of activation but also reflects the strong interaction between Na^+ and the carbon matrix [44]. The SEM–EDX results provide qualitative evidence of enhanced porosity, reduced impurities, and increased surface functionality after NaOH activation, which are consistent with the improved adsorption performance observed experimentally.

3.2.2 FTIR

FTIR analysis was performed to observe the functional groups of the prepared adsorbent. Figure 6 shows the FTIR spectra of the adsorbent before activation (MSC) and after activation (MSAC). Figure 6 shows the FTIR spectra of melinjo shell waste carbon before activation (MSC, Figure 6(A)) and after chemical activation with 2 M NaOH (MSAC, Figure 6(B)). Both materials display a broad absorption in the region of ~3628–3200 cm^{-1}, attributable to O–H stretching of hydroxyl groups and adsorbed water. The band near 2880–2920 cm^{-1} corresponds to aliphatic C–H stretching, while the peak at 1763–1707 cm^{-1} indicates oxygen–containing surface groups, particularly carbonyls (C=O) such as carboxylic acids, esters, or lactones. Aromatic C=C skeletal vibrations appear at ~1506 cm^{-1}, C–O stretching of phenolic or ether groups is observed at 1260–1220 cm^{-1}, and out–of–plane aromatic C–H bending vibrations are evident at 826–760 cm^{-1}. These functional groups (O–H, C=O, C–O) are commonly present on activated carbons and are relevant to surface reactivity [45]–[47].

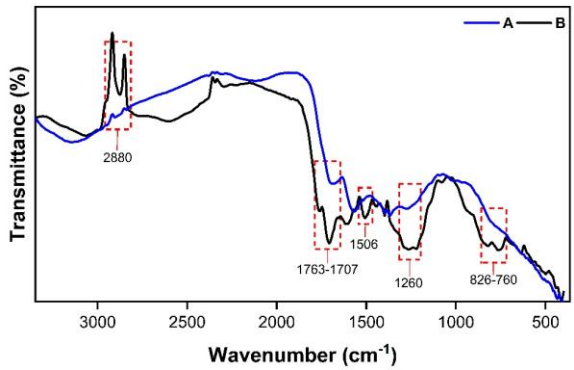

Figure 6: FTIR spectra of: (A) carbonized melinjo shell waste carbon before activation (MSC, black) and (B) carbonized melinjo shell waste carbon after activation under optimal conditions (MSAC, blue).

Upon activation, MSAC exhibits notable changes. The O–H stretching band becomes broader and slightly shifted (to 3612 cm^{-1}), suggesting enhanced hydrogen bonding and relative enrichment of hydroxyl functionalities on the surface. The intensity of aliphatic C–H and some carbonyl bands decreases, consistent with the removal of residual tars, aliphatic, and unstable oxygen species during NaOH treatment and subsequent washing [48]. Meanwhile, aromatic C=C and C–O bands become relatively more pronounced, reflecting the exposure of a more condensed aromatic carbon backbone enriched with stable oxygen–containing groups.

The presence of a band in the range of 1763–1707 cm^{-1} further confirms the existence of –COOH groups on the MSAC surface. These carboxylic groups can ionize to form $–COO^-$ species at pH values above approximately 5, contributing to the negative surface charge and promoting electrostatic attraction with cationic methylene blue molecules. At lower pH, these groups remain protonated (–COOH), reducing their ability to bind MB electrostatically, which aligns well with the observed lower adsorption capacity and removal efficiency under acidic conditions (Figure 8).

It is also possible that NaOH treatment converts some surface hydroxyl or carboxyl groups into sodium carboxylates or phenolates. Even after washing to neutrality, a fraction of these sodium–containing functionalities may remain bound to the carbon surface, which is consistent with the EDX results (Figure 5(D)) showing increased sodium content after activation. The FTIR spectral modifications confirm

that NaOH activation not only cleans and restructures the carbon matrix but also enhances the availability of oxygen–containing functional groups (O–H, C=O, C–O), thereby improving the adsorption performance of MSAC toward MB. This transformation may further enhance the density of oxygenated active sites, improving the adsorptive affinity toward MB.

These FTIR observations, in conjunction with SEM–EDX findings, qualitatively support the hypothesis that NaOH activation increases surface functionality and porosity. Although quantitative surface area data (BET) were not obtained, the combined evidence strongly suggests that the enhancement in adsorption capacity arises from both the physical development of the pore network and the enrichment of active oxygenated surface sites.

3.3 *Adsorption study*

3.3.1 Effect of contact time

Contact time is a critical factor influencing adsorption efficiency, as it determines the duration required for activated carbon to interact with MB molecules. As shown in Figure 7, the adsorption capacity of MSAC increased sharply within the first 35 min, reaching a %R and Q_e of 99.44% and 59.664 mg/g, respectively. This rapid uptake can be attributed to the abundance of unoccupied active sites and the strong driving force for mass transfer at the early adsorption stage. Similar results were reported by Julinawati *et. al.,* and Kadimpati *et. al*., who observed that MB adsorption increased significantly during the initial contact period (up to the first hour), followed by a gradual decline in adsorption capacity due to surface saturation [5], [49].

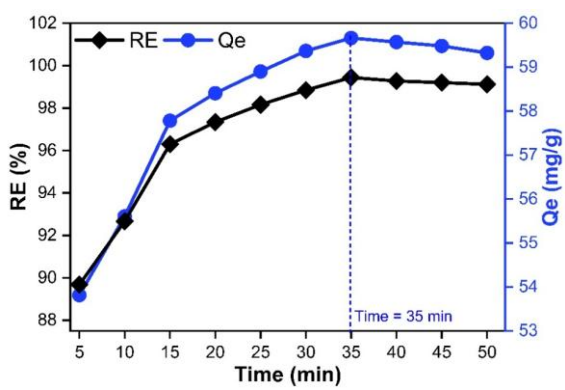

Figure 7: Effect of contact time for MB adsorption by MSAC. Experimental condition: MB initial concentration 200 ppm, volume 0.015 L, adsorbent dosage 0.05 g, neutral pH, at 25 °C.

Beyond 35 min, the adsorption capacity of MSAC slightly decreased, which may be associated with desorption phenomena or the attainment of dynamic equilibrium, where most active sites were already occupied and competition between adsorbed and free MB molecules occurred. Ozcan *et. al.,* also noted a comparable trend, who emphasized that prolonged contact time does not necessarily enhance adsorption performance but may lower efficiency due to repulsive interactions and site saturation [50]. These findings suggest that the optimum contact time for MB adsorption onto MSAC is approximately 35 min.

3.3.2 Effect of pH

The pH of the solution is a decisive factor influencing the ionization state of surface functional groups on the adsorbent as well as the speciation and charge distribution of the dye molecules. As illustrated in Figure 8, the adsorption of MB by MSAC was strongly affected by solution pH. The highest adsorption capacity (59.69 mg/g) and removal efficiency (>99%) were observed at pH 7. At acidic conditions (pH < 7), the abundance of protons (H^+) competed with the cationic MB molecules for negatively charged adsorption sites (e.g., oxygen–containing functional groups such as –OH and –COOH). This competition suppressed the electrostatic attraction between MB and MSAC, leading to lower adsorption capacities. Similar inhibitory effects of protonation under acidic conditions have been reported for cationic dye adsorption onto activated carbons and biomass–derived adsorbents [49].

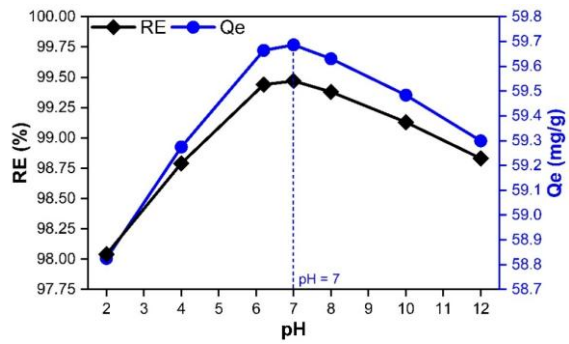

Figure 8: Effect of pH of the adsorbate on MB adsorption by MSAC. Experimental conditions: MB initial concentration 200 ppm, solution volume 0.015 L, adsorbent dosage 0.05 g, contact time 35 min, and temperature 25 °C.

A gradual decline in adsorption capacity was observed at alkaline conditions (pH > 7). This may be attributed to the increasing concentration of hydroxide ions (OH^-), which interact with MB cations in solution and reduce their effective interaction with the negatively charged surface of MSAC. Additionally, strong OH^- competition may destabilize dye molecules and hinder their access to pore channels, lowering adsorption efficiency [51].

This behavior differs from that reported in a previous study, which observed maximum MB adsorption at more alkaline pH values [52]. The discrepancy can be explained by the specific surface chemistry of MSAC: NaOH activation introduces abundant surface hydroxyl and sodium–containing groups (e.g., –ONa, Na–O–C) that partially neutralize the negative surface charge at high pH. Consequently, beyond neutral pH, the electrostatic driving force between the cationic MB and the MSAC surface weakens due to charge screening by excess Na^+ ions and intense OH^- competition. Moreover, the possible aggregation or hydrolysis of MB molecules in highly alkaline conditions can further decrease their availability for adsorption. Therefore, the optimal adsorption observed at pH 7 corresponds to a condition in which protonation and deprotonation are balanced, thereby maximizing both electrostatic and π–π interactions between MB and the carbon surface.

This observation is consistent with previous findings on the pH–dependent adsorption behavior of cationic dyes on alkali–activated carbons [6], [53], [54]. It is acknowledged that determining the point of zero charge (pHPZC) of MSAC would provide direct evidence of surface charge behavior and further substantiate the proposed electrostatic interaction mechanism. Nevertheless, the observed pH–dependent adsorption trend and the established surface chemistry of NaOH-activated carbons strongly support the involvement of electrostatic attraction between the negatively charged surface and cationic MB molecules.

These findings confirm that the adsorption of MB by MSAC is highly pH–dependent, with neutral conditions providing the most favorable environment for maximizing uptake. Building upon this optimum pH, it is also essential to evaluate the effect of the initial dye concentration, since the driving force for mass transfer and the degree of surface site saturation are directly influenced by solute loading in solution.

3.3.3 Effect of initial concentration

The initial concentration of an adsorbate is a critical factor influencing the driving force for mass transfer between the aqueous phase and the adsorbent surface. As shown in Figure 9, the adsorption performance of MSAC toward MB varied with initial dye concentration.

At lower concentrations (150 ppm), MSAC exhibited a high removal efficiency of approximately 98%. The percentage removal reached its maximum (99.44%) at 200 ppm, indicating that most MB molecules were effectively captured by the available active sites. However, a slight decline was observed at 250 ppm, likely due to the limited number of accessible adsorption sites relative to the excess dye molecules in solution.

The adsorption capacity increased from 55.6 mg/g at 150 ppm to 73.7 mg/g at 200 ppm, but then decreased slightly to 59 mg/g at 250 ppm. This seemingly anomalous trend can be explained by several interrelated factors. At higher dye concentrations, aggregation of MB molecules in solution or within pore entrances can restrict diffusion and access to inner adsorption sites. In addition, multilayer formation or steric hindrance may occur on the carbon surface, leading to partial pore blockage and reduced site utilization. Electrostatic repulsion among cationic MB molecules at the surface may also limit further adsorption once the surface approaches saturation.

Therefore, the observed decrease in Q_e at 250 ppm does not imply a reduction in adsorption potential, but rather indicates a diffusion-limited regime in which equilibrium is reached before all sites are fully saturated. Similar concentration–dependent trends have been reported for MB adsorption on NaOH–activated carbons and other biomass–derived adsorbents [55], [56], [57].

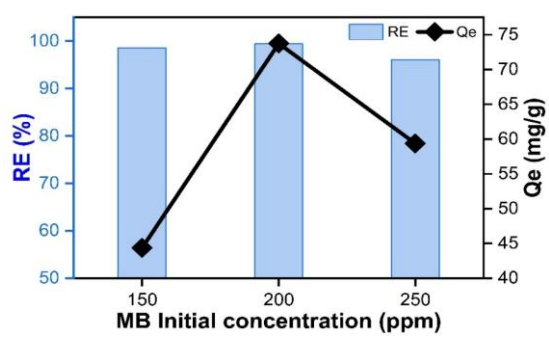

Figure 9: Effect of initial concentration of MB adsorption by MSAC. Experimental condition: contact time 35 min, volume 0.015 L, adsorbent dosage 0.05 g, neutral pH, at 25 °C.

Interestingly, some previous studies have reported an opposite trend, where adsorption capacity continues to increase with higher initial dye concentrations. For instance, Dolas [58] observed that the adsorption capacity of waste pepper stalks-based activated carbon for MB increased from 50.216 mg/g at 50 ppm to 104.20 mg/g at 250 ppm, attributing this to enhanced diffusion rates and a higher probability of molecular collision at greater solute concentrations. Similarly, Julinawati *et. al.,* [5] found a linear correlation between dye concentration and adsorption efficiency, indicating that higher concentration can strengthen the driving force for mass transfer. These variations emphasize that the behavior depends strongly on the adsorbent structure and surface chemistry. In comparison, the slight decline in our study at 250 ppm likely arises from the unique structural and diffusional properties of MSAC, in which excessive dye aggregation or pore restriction limits further uptake.

These results indicate that at lower MB concentrations, the active sites of MSAC were sufficient to adsorb nearly all dye molecules present in solution. This explains the high removal efficiency (R) observed under these conditions. However, at elevated concentrations, the fixed number of active sites on MSAC could not capture the excess MB molecules, resulting in a decrease in removal efficiency (R) despite increased total dye loading. The optimal initial concentration for MB adsorption by MSAC was 200 ppm, reflecting a balance between the mass-transfer driving force and active-site accessibility. In the subsequent section, equilibrium data were analyzed using isotherm models such as Langmuir, Freundlich, Sips, and Temkin to further elucidate the adsorption mechanism and quantify the affinity between MB and MSAC.

3.3.4 Adsorption isotherms studies

The equilibrium adsorption data of MB onto MSAC were analyzed using four non-linear isotherm models, namely Langmuir, Freundlich, Temkin, and Sips (Figure 10, Table 1). Among these, the Langmuir model exhibited the best fit to the experimental data (R^2 = 0.963), indicating that MB adsorption predominantly followed monolayer coverage on a relatively homogeneous surface. The calculated maximum adsorption capacity (Q_{max}) from the Langmuir model was 148.214 mg/g, which is significantly higher than many other agricultural waste-derived adsorbents. For instance, *Spathodea campanulata*, coconut husk, coal, and areca residue biochar–based activated carbons exhibited adsorption capacities of 86.21, ~15.5, 15, and 127.2 mg/g, respectively [43], [59]–[61]. Even in our previous study using NaCl activation, melinjo shell waste–based carbon only reached 62.5 mg/g [31]. These comparisons confirm that NaOH activation substantially improves the adsorption performance of melinjo shell waste activated carbon.

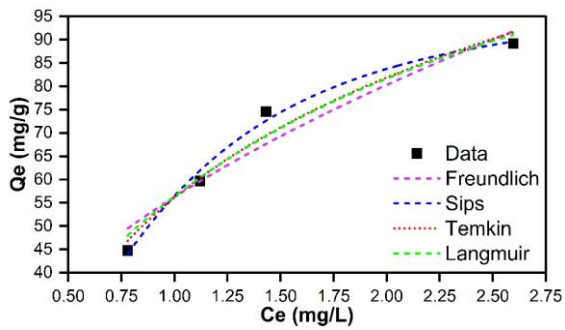

Figure 10: Isotherm fitting non-linear model of MB removal using MSAC.

The Freundlich model provided a relatively good fit (R^2 = 0.930), with an adsorption intensity factor (n = 1.947) within the favorable range (1 < n < 10), indicating heterogeneous surface adsorption and the possibility of multilayer uptake. The high KF value (56.252 mg/g) further suggests a strong interaction between MB molecules and the MSAC surface, consistent with both chemisorption and physisorption mechanisms. The Temkin model also showed reasonable agreement (R^2 = 0.950), reflecting a decrease in the heat of adsorption with surface coverage, which implies that adsorbate–adsorbate interactions and surface heterogeneity play a role.

The Temkin constant (B = 85.655 mg/g) supports moderate binding energy, aligning with electrostatic interactions between cationic MB and oxygenated groups on MSAC. The Sips model, which combines Langmuir and Freundlich features, exhibited the lowest correlation (R^2 = 0.913) compared to the other models, suggesting that while surface heterogeneity exists, monolayer adsorption dominates under the studied conditions. The Sips exponent (n_S = 2.004), greater than 1, also indicates favorable adsorption, but the relatively lower fit suggests that the model provides no significant advantage over Langmuir in describing this system.

Table 1: Isotherm model for MB adsorption using MSAC.

Isotherm model	Parameter	Unit	Value
Freundlich	K_F	mg/g	56.252
$q_e = K_F C_e^{\frac{1}{n}}$	n	–	1.947
	R^2	–	0.930
Langmuir	Q_{max}	mg/g	148.214
$q_e = \frac{Q_m K_L C_e}{1 + K_L C_e}$	K_l	L/mg	0.614
	R^2	–	0.963
Temkin	B	mg/g	85.655
$q_e = B \times Ln(AC_e)$	A	L/mg	4.520
	R^2	–	0.950
Sips	Q_{ms}	mg/g	99.752
$q_e = \frac{Q_{ms} K_s C_e^{ns}}{1 + K_s C_e^{ns}}$	K_s	L/mg	1.142
	n_s	–	2.004
	R^2	–	0.913

K_F, Freundlich constant related to adsorption capacity (mg/g); n, Freundlich intensity parameter indicating adsorption favorability; Q_{max}, maximum monolayer adsorption capacity (mg/g); K_l, Langmuir adsorption equilibrium constant (L/mg); B, Temkin constant related to adsorption heat (mg/g); A, Temkin equilibrium binding constant (L/mg); Q_{ms}, maximum adsorption capacity from the Sips model (mg/g); K_s, Sips equilibrium constant (L/mg); n_s, Sips model exponent indicating surface heterogeneity; R^2, correlation coefficient.

Table 2: Comparison of Q_{max} of MB adsorption using various adsorbents.

Adsorbent-Based–AC	Activation Method	Chemical Activator	Q_{max} (mg/g)	Ref.
Coconut husk	Physical and chemical	H_3PO_4	~15.5	[43]
Bamboo	Chemical	KOH	67.5	[62]
spathodea campanulate	Chemical and thermal	H_3PO_4	86.2	[59]
Coal	Chemical	KOH	15.0	[60]
Areca residue biochar	Chemical	NaOH	127.2	[61]
Peanut stick wood	Chemical	HCl and HNO_3	2.6	[63]
Sugarcane bagasse	Chemical	KOH	136.5	[64]
coconut shell	Chemical	NaOH	50 – 100	[65]
Melinjo shell waste	Chemical	NaCl	62.5	[31]
Glucose	Chemical	KOH	61	[66]
G. *gnemon* shell waste	Chemical	NaOH	148.214	This work

The non–linear isotherm analysis confirms that the adsorption of MB onto MSAC is primarily governed by Langmuir–type monolayer chemisorption, facilitated by electrostatic interactions and π–π electron donor–acceptor interactions between the aromatic structures of MB and the delocalized π–electron system of the activated carbon. Meanwhile, the partial fit of the Freundlich and Temkin models suggests additional contributions from surface heterogeneity and weaker multilayer interactions at higher concentrations. This dual adsorption mechanism, dominated by Langmuir behavior, underpins the remarkably high adsorption capacity of MSAC and demonstrates its strong potential as an efficient and sustainable adsorbent for dye–polluted wastewater.

Overall, the isotherm analysis demonstrates that NaOH activation effectively increases surface porosity and introduces oxygen–containing functional groups, thereby enhancing the affinity of MSAC toward cationic dyes such as methylene blue. The predominant Langmuir behavior confirms that adsorption occurs mainly through monolayer chemisorption involving electrostatic attraction, ion exchange, and possible π–π interactions. At the same time, the partial Freundlich contribution suggests some degree of multilayer physisorption at higher concentrations. Such a dual mechanism, dominated by Langmuir–type interactions, underpins the remarkably high adsorption capacity of MSAC (148.214 mg/g), which substantially exceeds that of many other agricultural waste–derived adsorbents (Table 2). This highlights the superior potential of MSAC as a cost–effective and sustainable material for dye–laden wastewater treatment. To further verify the adsorption mechanism and evaluate the rate–limiting step, kinetic studies using pseudo-first-order (PFO) and pseudo–second–order (PSO) models were performed.

Although direct adsorption tests using unactivated MSC were not performed, the comparative characterization results (SEM–EDX and FTIR) clearly demonstrate the significant improvement in surface morphology, elemental composition, and functional group enrichment after NaOH activation. These findings strongly indicate that the enhanced adsorption performance of MSAC primarily arises from the activation–induced development of porosity and active surface sites. Future studies should include a direct adsorption comparison between MSC and MSAC to quantitatively confirm this enhancement.

3.3.5 Adsorption kinetics studies

To further elucidate the MB adsorption mechanism onto MSAC, the kinetic data were analyzed using non–linear pseudo–first–order (PFO) and pseudo–second–order (PSO) (Table 3, Figure 11). The PFO model yielded an R^2 value of 0.988 and an estimated adsorption capacity (58.192 mg/g) lower than the experimental value (59.67 mg/g), suggesting that PFO is not the most suitable model to represent the MB uptake process. In contrast, the PSO model exhibited

an excellent correlation (R^2 = 0.999) and provided a calculated adsorption capacity (60.378 mg/g) close to the experimental value. This superior agreement indicates that the adsorption of MB onto MSAC is predominantly governed by chemisorption, involving valence forces through electron sharing or exchange between MB molecules and surface functional groups. This behavior reflects the surface heterogeneity of MSAC, where a distribution of activation energies governs the adsorption process.

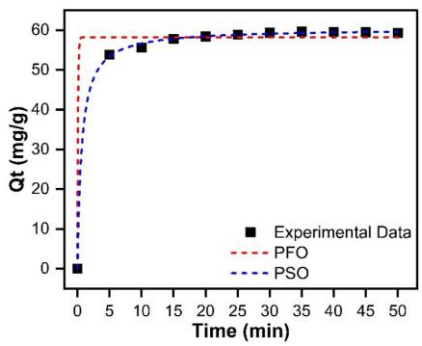

Figure 11: Adsorption kinetic model of MB removal using MSAC.

The dominance of the PSO model is fully consistent with the Langmuir isotherm results (Q_{max} = 148.214 mg/g, R^2 = 0.963), confirming that MB adsorption on MSAC mainly occurs via monolayer chemisorption on a relatively homogeneous surface. Comparable behaviors have been reported for other agricultural waste–derived carbons. For instance, activated carbons derived from areca residue biochar [61], peanut stick wood [63], and olive pits [67] also demonstrated Langmuir–PSO dominance, attributed to abundant oxygenated surface functionalities that enhance electrostatic binding with cationic dyes. The present study, however, reports a notably higher adsorption capacity (148.214 mg/g), underscoring the efficiency of MSAC in dye removal compared with many other biomass–derived adsorbents.

Table 3: Adsorption kinetics parameters of MB removal using MSAC.

Kinetic Models	Parameters	Value
Pseudo–first–order	Q_e	58.192 mg/g
$q_t = q_e\,(1 - e^{-k_1 t})$	K_1	11.861 1/min
	R^2	0.988
Pseudo–second–order	Q_e	60.378 mg/g
$q_t = \frac{k_2\, q_e^2\, t}{1 + k_2\, q_e\, t}$	K_2	0.025 g/(mg.min)
	R^2	0.999

Q_e, equilibrium adsorption capacity (mg/g); K_1, pseudo–first–order rate constant (1/min); K_2, pseudo–second–order rate constant (g/(mg.min)); R^2, correlation coefficient.

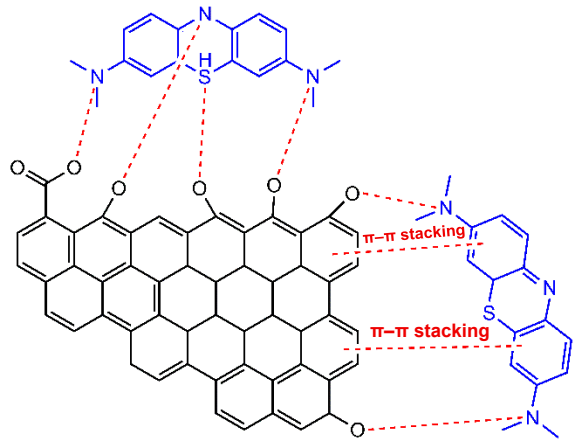

Figure 12: Proposed adsorption mechanism of MB onto MSAC.

The coupled isotherm–kinetic analysis confirms that MB adsorption onto MSAC is primarily a chemisorption–driven process occurring on homogeneous active sites. The process is characterized by rapid uptake and high capacity, rendering MSAC a highly promising adsorbent for wastewater remediation. A schematic representation of the proposed adsorption mechanism, highlighting electrostatic attraction, π–π interactions, and site heterogeneity, is illustrated in Figure 12.

The overall findings demonstrate that NaOH activation significantly enhances MSAC adsorption efficiency toward MB dye. While these results confirm the strong adsorption potential of MSAC for MB removal, further evaluation of its long-term performance remains necessary. In particular, desorption and reusability studies were not performed in the present work. Such experiments are essential to assess the regeneration potential and operational stability of MSAC in practical wastewater treatment systems. Future investigations should therefore include cyclic adsorption–desorption experiments using mild eluents, such as ethanol, NaCl, or dilute acids, to evaluate the stability, regeneration efficiency, and possible structural degradation of MSAC after repeated use. Including these data would provide valuable insights into the economic feasibility and sustainability of the adsorbent.

4 Conclusions

This study demonstrated the efficient methylene blue (MB) adsorption from aqueous solution using NaOH-activated carbon derived from melinjo shell waste (MSAC). This is the first reported study utilizing

NaOH activation for *G. gnemon* shell waste biomass, highlighting its novelty as a sustainable precursor for high-performance activated carbon. Optimal adsorption conditions were achieved rapidly at pH 7 and 35 min, even at a relatively high initial concentration of 200 ppm, making MSAC suitable for treating dye-rich wastewater. The maximum adsorption capacity reached 148.214 mg/g, which is more than twice that of previously reported G. *gnemon*–based carbons activated by physical or NaCl treatment. Equilibrium data were best described by the Langmuir isotherm, indicating monolayer adsorption on a homogeneous surface. Kinetic studies revealed that the adsorption process followed the pseudo-second-order (PSO) model, suggesting chemisorption as the dominant mechanism through electron exchange and strong interactions between MB molecules and oxygenated functional groups of MSAC. The results confirm that NaOH activation significantly enhances pore development and surface reactivity, leading to superior dye adsorption efficiency. Overall, MSAC shows promise as a low-cost, fast-acting, and high-capacity adsorbent for dye-laden wastewater treatment. Future work should include pHPZC and BET surface area analyses to quantitatively confirm the surface charge behavior and porosity characteristics of MSAC, as well as adsorption–desorption cycle experiments to evaluate its regeneration potential and long-term performance.

Acknowledgments

The authors would like to express their sincere gratitude to Universitas Syiah Kuala and the Ministry of Research, Technology, and Higher Education of the Republic of Indonesia for financial support.

Author Contributions

L.L.: Conceptualization, methodology, validation, resources, data curation, and funding acquisition; A.H.: Formal analysis, investigation; A.A.K.; writing an original draft, writing—reviewing and editing, and visualization. K.S.: Supervision and writing—reviewing and editing. All authors have read and agreed to the published version of the manuscript.

Conflict of Interest

The authors declare that they have no known competing financial interests or personal relationships that could have appeared to influence the work reported in this paper.

Declaration of generative AI and AI-assisted technologies in the writing process

The authors utilized the ChatGPT tool to enhance the language and readability of the manuscript.

References

[1] B. J. Singh, A. Chakraborty, and R. Sehgal, "A systematic review of industrial wastewater management: Evaluating challenges and enablers," *Journal of Environmental Management*, vol. 348, Dec. 2023, Art. no. 119230, doi: 10.1016/j.jenvman.2023.119230.

[2] M. M. Islam, A. R. Aidid, J. N. Mohshin, H. Mondal, S. Ganguli, and A. K. Chakraborty, "A critical review on textile dye-containing wastewater: Ecotoxicity, health risks, and remediation strategies for environmental safety," *Clean Chemical Engineering*, vol. 11, Dec. 2025, Art. no. 100165, doi: 10.1016/j.clce.2025.100165.

[3] Kusumlata, B. Ambade, A. Kumar, and S. Gautam, "Sustainable solutions: Reviewing the future of textile dye contaminant removal with emerging biological treatments," *Limnological Review*, vol. 24, no. 2, pp. 126–149, Apr. 2024, doi: 10.3390/limnolrev24020007.

[4] P. O. Oladoye, T. O. Ajiboye, E. O. Omotola, and O. J. Oyewola, "Methylene blue dye: Toxicity and potential elimination technology from wastewater," *Results in Engineering*, vol. 16, Dec. 2022, Art. no. 100678, doi: 10.1016/j.rineng.2022.100678.

[5] J. Julinawati, R. Rahmi, Z. P. Karnain, I. Mustafa, K. MZ, M. Farida, A. A. Kacaribu, "Preparation of magnetic-activated biocarbon composite from Red Algae for dye removal from water," *Journal of Ecological Engineering*, vol. 26, no. 8, pp. 67–85, Aug. 2025, doi: 10.12911/22998993/203746.

[6] A. H. Birniwa et al., "Adsorption behavior of methylene blue cationic dye in aqueous solution using polypyrrole-polyethylenimine nano-adsorbent," *Polymers (Basel)*, vol. 14, no. 16, Aug. 2022, Art. no. 3362, doi: 10.3390/polym14163362.

[7] S. H. Siddiqui, M. K. Uddin, R. Isaac, and O. F. Aldosari, "An effective biomass for the

adsorption of methylene blue dye and treatment of river water," *Adsorption Science & Technology*, vol. 2022, 2022, Art. no. 4143138, doi: 10.1155/2022/4143138.

[8] C. Yahya, T. Choong, F. Li, W. Ghani, F. Aziz, and S. Jamil, "Tailing ash for the removal of methylene blue from aqueous solutions by batch adsorption," *Processes*, vol. 11, Aug. 2023, Art. no. 2282, doi: 10.3390/pr11082282.

[9] N. H. Torres, B. S. Souza, L. F. R. Ferreira, Á. S. Lima, G. N. dos Santos, and E. B. Cavalcanti, "Real textile effluents treatment using coagulation/flocculation followed by electrochemical oxidation process and ecotoxicological assessment," *Chemosphere*, vol. 236, Jul. 2019, Art. no. 124309, doi: 10.1016/j.chemosphere.2019.07.040.

[10] A. A. Kacaribu, Y. Aisyah, Febriani, and Darwin, "Development of wastewater treatment methods for palm oil mill effluent (POME): A comprehensive review," *Resources, Chemicals and Materials*, vol. 5, Dec. 2025, Art. no. 100130, doi: 10.1016/j.recm.2025.100130.

[11] G. A. Ismail and H. Sakai, "Review on the effect of different types of dyes on advanced oxidation processes (AOPs) for textile color removal," *Chemosphere*, vol. 291, Jan. 2022, Art. no. 132906, doi: 10.1016/j.chemosphere.2021.132906.

[12] A. Lanzetta et al., "Ozonation processes for color removal from urban and leather tanning wastewater," *Water*, vol. 15, July 2023, Art. no. 2362, doi: 10.3390/w15132362.

[13] E.-S. Z. El-Ashtoukhy and Y. O. Fouad, "Liquid–liquid extraction of methylene blue dye from aqueous solutions using sodium dodecylbenzenesulfonate as an extractant," *Alexandria Engineering Journal*, vol. 54, pp. 77–81, 2015, doi: 10.1016/j.aej.2014.11.007.

[14] Lelifajri, M. A. Nawi, S. Sabar, Supriatno, and W. I. Nawawi, "Preparation of immobilized activated carbon–polyvinyl alcohol composite for the adsorptive removal of 2,4-dichlorophenoxyacetic acid," *Journal of Water Process Engineering*, vol. 25, pp. 269–277, 2018, doi: 10.1016/j.jwpe.2018.08.012.

[15] B. G. Fouda-Mbanga, O. Onotu, and Z. Tywabi-Ngeva, "Advantages of the reuse of spent adsorbents and potential applications in environmental remediation: A review," *Green Analytical Chemistry*, vol. 11, 2024, Art. no. 100156, doi: 10.1016/j.greeac.2024.100156.

[16] H. Fathana, Rahmi, M. Adlim, S. Lubis, and M. Iqhrammullah, "Sugarcane bagasse-derived cellulose as an eco-friendly adsorbent for azo dye removal," *International Journal of Design & Nature and Ecodynamics*, vol. 18, Jan. 2023, no. 1, pp. 11–20, doi: 10.18280/ijdne.180102.

[17] A. A. Kacaribu, Y. Aisyah, Febriani, and Darwin, "The development of green polylactic acid (PLA) composites for the wastewater treatment process – A review," *Engineering Transactions*, vol. 73, Sept. 2025, pp. 485–524, doi: 10.24423/engtrans.3534.2025.

[18] A. A. Kacaribu and D. Darwin, "Biotechnological lactic acid production from low-cost renewable sources via anaerobic microbial processes," *BioTechnologia*, vol. 105, no. 2, pp. 179–194, 2024, doi: 10.5114/bta.2024.139757.

[19] R. Rahmi, L. Lelifajri, F. Fathurrahmi, H. Fathana, and M. Iqhrammullah, "Preparation and characterization of PEGDE-EDTA-modified magnetic chitosan microsphere as an eco-friendly adsorbent for methylene blue removal," *South African Journal of Chemical Engineering*, vol. 43, pp. 296–302, 2023, doi: 10.1016/j.sajce.2022.11.009.

[20] H. V. T. Luong, T. P. Le, T. L. T. Le, H. G. Dang, and T. B. Q. Tran, "A graphene oxide-based composite granule for methylene blue separation from aqueous solution: Adsorption, kinetics and thermodynamic studies," *Heliyon*, vol. 10, Art. no. e28648, 2024, doi: 10.1016/j.heliyon.2024.e28648.

[21] J. B. Njewa and V. O. Shikuku, "Recent advances and issues in the application of activated carbon for water treatment in Africa: A systematic review (2007–2022)," *Applied Surface Science Advances*, vol. 18, Art. no. 100501, 2023, doi: 10.1016/j.apsadv.2023.100501.

[22] N. A. Basha, T. Rathinavel, and H. Sridharan, "Activated carbon from coconut shell: Synthesis and its commercial applications—A recent review," *Applied Science and Engineering Progress*, vol. 37, no. 6, 2022, doi: 10.14416/j.asep.2022.07.001.

[23] R. K. Mishra, B. Singh, and B. Acharya, "A comprehensive review on activated carbon from pyrolysis of lignocellulosic biomass: An application for energy and the environment," *Carbon Resources Conversion*, vol. 7, Art. no. 100228, 2024, doi: 10.1016/j.crcon.2024.100228.

[24] K. Malini, D. Selvakumar, and N. S. Kumar,

"Activated carbon from biomass: Preparation, factors improving basicity and surface properties for enhanced CO_2 capture capacity – A review," *Journal of CO_2 Utilization*, vol. 67, Art. no. 102318, 2023, doi: 10.1016/j.jcou.2022.102318.

[25] T. Alfatah, E. M. Mistar, and M. D. Supardan, "Porous structure and adsorptive properties of activated carbon derived from *Bambusa vulgaris striata* by two-stage KOH/NaOH mixture activation for Hg^{2+} removal," *Journal of Water Process Engineering*, vol. 43, 2021, Art. no. 102294, doi: 10.1016/j.jwpe.2021.102294.

[26] O. O. Barah, S. N. Nnamchi, K. C. Onyelowe, M. S. Dennison, and E. B. O. Olotu, "Effects of NaOH and KOH activator agents on the aluminization process," *Advanced Metamaterials*, vol. 1, no. 2, 2025, doi: 10.1007/s44468-025-00001-1.

[27] T. Somsiripan and C. Sangwichien, "Enhancement of adsorption capacity of methylene blue, malachite green, and rhodamine B onto KOH-activated carbon derived from oil palm empty fruit bunches," *Arabian Journal of Chemistry*, vol. 16, 2023, Art. no. 105270, doi: 10.1016/j.arabjc.2023.105270.

[28] S. M. Anisuzzaman, R. F. Mansa, M. Rajin, N. M. Ismail, M. Sundang, and N. S. A. M. Sazuli, "The activated carbon produced from bamboo biochar and its application as methylene blue dye removal from wastewater," in *Nutrients and Colorants in Wastewater*, Amsterdam, Netherlands: Elsevier, 2025, pp. 359–392, doi: 10.1016/B978-0-443-21701-2.00019-2.

[29] J. Georgin, G. L. Dotto, M. A. Mazutti, and E. L. Foletto, "Preparation of activated carbon from peanut shell by conventional pyrolysis and microwave irradiation-pyrolysis to remove organic dyes from aqueous solutions," *Journal of Environmental Chemical Engineering*, vol. 4, pp. 266–275, 2016, doi: 10.1016/j.jece.2015.11.018.

[30] Lelifajri, Rahmi, Supriatno, Susilawati, and A. S. M. Indarum, "Study on methylene blue dye adsorption in aqueous solution by heat-treated *Gnetum gnemon* shell waste particles as low-cost adsorbent," in *AIP Conference Proceedings*, 2020, p. 020012, doi: 10.1063/5.0001358.

[31] Lelifajri, Rahmi, Supriatno, and Susilawati, "Preparation of activated carbon from *Gnetum gnemon* shell waste by furnace–NaCl activation for methylene blue adsorption," *Journal of Physics: Conference Series*, vol. 1940, 2021, Art. no. 012040, doi: 10.1088/1742-6596/1940/1/012040.

[32] A. Setiawan, Z. Jalil, S. Nurjannah, S. Riskina, and M. Muhammad, "Role of activated carbon from Arabica coffee waste in enhancing the dehydrogenation properties of magnesium hydride (MgH_2) for hydrogen storage," *Applied Science and Engineering Progress*, vol. 18, no. 4, Oct. 2025, Art. no. 7741 doi: 10.14416/j.asep.2025.05.010.

[33] R. J. P. Latiza and R. V. Rubi, "Circular economy integration in 1G+2G sugarcane bioethanol production: Application of carbon capture, utilization and storage, closed-loop systems, and waste valorization for sustainability," *Applied Science and Engineering Progress*, vol. 18. no. 1, Jul. 2025, Art. no. 7448, doi: 10.14416/j.asep.2024.07.005.

[34] A. A. Kacaribu, R. Rahmi, J. Julinawati, H. Fathana, M. Reza, and M. Iqhrammullah, "Preparation and characterization of cellulose film from velvet tamarind rind (*Dialium indum* L.) for food packaging," *Applied Science and Engineering Progress*, vol. 18, no. 3, Jul. 2025, Art. no. 7724, doi: 10.14416/j.asep.2025.03.006.

[35] M. T. Vu, H.-P. Chao, T. Van Trinh, T. T. Le, C.-C. Lin, and H. N. Tran, "Removal of ammonium from groundwater using NaOH-treated activated carbon derived from corncob wastes: Batch and column experiments," *Journal of Cleaner Production*, vol. 180, pp. 560–570, Apr. 2018, doi: 10.1016/j.jclepro.2018.01.104.

[36] N. Samghouli, I. Bencheikh, K. Azoulay, S. Jansson, and S. El Hajjaji, "Mechanistic and reactional activation study of carbons destined for emerging pharmaceutical pollutant adsorption," *Environmental Monitoring and Assessment*, vol. 197, Feb. 2025, Art. no. 259, doi: 10.1007/s10661-025-13685-4.

[37] A. Khamkeaw, W. Sanprom, and M. Phisalaphong, "Activated carbon from bacterial cellulose by potassium hydroxide activation as an effective adsorbent for removal of ammonium ion from aqueous solution," *Case Studies in Chemical and Environmental Engineering*, vol. 8, Dec. 2023, Art. no. 100499, doi: 10.1016/j.cscee.2023.100499.

[38] Y. Chen et al., "Study on the properties of activated carbon based on activation process and NaOH modification," *Advanced Bamboo Science*, vol. 12, Aug. 2025, Art. no. 100186, doi: 10.1016/j.bamboo.2025.100186.

[39] SNI, *Arang Aktif Teknis (Activated Carbon)*, Indonesian National Standard-SNI 06-3730-1995, Jakarta, 1995.

[40] Y. Zhang et al., "Redefining the roles of alkali activators for porous carbon," *Chemical Science*, vol. 16, pp. 2034–2043, 2025, doi: 10.1039/D4SC07145J.

[41] M. A. Kononova, N. V. Vorob'ev-Desyatovskii, R. I. Ibragimova, and S. A. Kubyshkin, "Effect of inorganic compounds in the activated carbon phase and in solution on the adsorption of gold(I) cyanide complex," *Russian Journal of Applied Chemistry*, vol. 82, pp. 173–182, 2009, doi: 10.1134/S1070427209020013.

[42] C. M. C. Silva, C. Maganinho, A. Mendes, J. Rocha, and I. Portugal, "Recovered carbon black: A comprehensive review of activation, demineralization, and incorporation in rubber matrices," *Carbon Resources Conversion*, vol. 7, May 2025, Art. no. 100334, doi: 10.1016/j.crcon.2025.100334.

[43] R. H. Khuluk, A. Rahmat, B. Buhani, and S. Suharso, "Removal of methylene blue by adsorption onto activated carbon from coconut shell (*Cocos nucifera* L.)," *Indonesian Journal of Science and Technology*, vol. 4, no. 2, pp. 229–240, 2019, doi: 10.17509/ijost.v4i2.18179.

[44] C. Saucier et al., "Microwave-assisted activated carbon from cocoa shell as adsorbent for removal of sodium diclofenac and nimesulide from aqueous effluents," *Journal of Hazardous Materials*, vol. 289, May 2015, pp. 18–27, doi: 10.1016/j.jhazmat.2015.02.026.

[45] J. Kawalerczyk, D. Dukarska, P. Antov, K. Stuper-Szablewska, D. Dziurka, and R. Mirski, "Activated carbon from coconut shells as a modifier of urea–formaldehyde resin in particleboard production," *Applied Sciences*, vol. 14, Art. no. 5627, 2024, doi: 10.3390/app14135627.

[46] E. H. Sujiono, D. Zabrian, Zurnansyah, Mulyati, V. Zharvan, Samnur, and N. A. Humairah, "Fabrication and characterization of coconut shell activated carbon using variation chemical activation for wastewater treatment application," *Results in Chemistry*, vol. 4, Jan. 2022, Art. no. 100291, doi: 10.1016/j.rechem.2022.100291.

[47] J. Saleem, Z. K. B. Moghal, S. Pradhan, and G. McKay, "High-performance activated carbon from coconut shells for dye removal: Study of isotherm and thermodynamics," *RSC Advances*, vol. 14, pp. 33797–33808, 2024, doi: 10.1039/D4RA06287F.

[48] S. Y. Yang, B. C. Bai, and Y. R. Kim, "Effective surface structure changes and characteristics of activated carbon with the simple introduction of oxygen functional groups by using radiation energy," *Surfaces*, vol. 7, pp. 12–25, 2024, doi: 10.3390/surfaces7010002.

[49] K. K. Kadimpati et al., "Design of innovative hybrid biochar prepared from marine algae and magnetite: Insights into adsorption performance and mechanism," *Chemical Engineering Research and Design*, vol. 201, pp. 218–227, 2024, doi: 10.1016/j.cherd.2023.11.053.

[50] D. O. Ozcan, M. C. Hendekçi, and B. Ovez, "Enhancing the adsorption capacity of organic and inorganic pollutants onto impregnated olive stone-derived activated carbon," *Heliyon*, vol. 10, Jun. 2024, Art. no. e32792, doi: 10.1016/j.heliyon.2024.e32792.

[51] E. Rápó and S. Tonk, "Factors affecting synthetic dye adsorption and desorption studies: A review of results from the last five years (2017–2021)," *Molecules*, vol. 26, Sep. 2021, Art. no. 5419, doi: 10.3390/molecules26175419.

[52] R. Salahshour, M. Shanbedi, and H. Esmaeili, "Methylene blue dye removal from aqueous media using activated carbon prepared by lotus leaves: Kinetic, equilibrium and thermodynamic study," *Acta Chimica Slovenica*, vol. 68, pp. 363–373, 2021, doi: 10.17344/acsi.2020.6311.

[53] F. Wei et al., "Insights into the pH-dependent adsorption behavior of ionic dyes on phosphoric acid-activated biochar," *ACS Omega*, vol. 7, Dec. 2022, pp. 46288–46302, doi: 10.1021/acsomega.2c04799.

[54] F. Ullah et al., "Adsorption performance and mechanism of cationic and anionic dyes by KOH-activated biochar derived from medical waste pyrolysis," *Environmental Pollution*, vol. 314, Dec. 2022, Art. no. 120271, doi: 10.1016/j.envpol.2022.120271.

[55] Y. Kuang, X. Zhang, and S. Zhou, "Adsorption of methylene blue in water onto activated carbon by surfactant modification," *Water*, vol. 12, Feb. 2020, Art. no. 587, doi: 10.3390/w12020587.

[56] N. Vasiljević, S. Panić, G. Tadić, J. Vuković, N. Novaković, and V. Mićić, "Investigation of the kinetics of the adsorption of methylene blue on activated carbon," *Engineering Proceedings*, vol. 99, no. 1, p. 4, 2025, doi: 10.3390/engproc2025099004.

[57] M. Abbas and M. Trari, "Adsorption behavior of

methylene blue onto activated coconut shells: Kinetic, thermodynamic, mechanism and regeneration of the adsorbent," *Dose-Response*, vol. 22, pp. 1–18, 2024, doi: 10.1177/15593258241290708.

[58] H. Dolas, "Activated carbon synthesis and methylene blue adsorption from pepper stem using microwave-assisted impregnation method: Isotherm and kinetics," *Journal of King Saud University – Science*, vol. 35, April 2023, Art. no. 102559, doi: 10.1016/j.jksus.2023.102559.

[59] D. Dimbo et al., "Methylene blue adsorption from aqueous solution using activated carbon of *Spathodea campanulata*," *Results in Engineering*, vol. 21, Mar. 2024, Art. no. 101910, doi: 10.1016/j.rineng.2024.101910.

[60] J. Wang, J. Ma, and Y. Sun, "Adsorption of methylene blue by coal-based activated carbon in high-salt wastewater," *Water*, vol. 14, Nov. 2022, Art. no. 3576, doi: 10.3390/w14213576.

[61] Y. Lu et al., "Adsorption characteristics and mechanism of methylene blue in water by NaOH-modified areca residue biochar," *Processes*, vol. 10, Dec. 2022, Art. no. 2729, doi: 10.3390/pr10122729.

[62] Q. Ge et al., "Removal of methylene blue by porous biochar obtained by KOH activation from bamboo biochar," *Bioresources and Bioprocessing*, vol. 10, Aug. 2023, Art. no. 51, doi: 10.1186/s40643-023-00671-2.

[63] M. Ghaedi, A. G. Nasab, S. Khodadoust, M. Rajabi, and S. Azizian, "Application of activated carbon as adsorbents for efficient removal of methylene blue: Kinetics and equilibrium study," *Journal of Industrial and Engineering Chemistry*, vol. 20, pp. 2317–2324, 2014, doi: 10.1016/j.jiec.2013.10.007.

[64] A. H. Jawad et al., "Microporous activated carbon developed from KOH-activated biomass waste: Surface mechanistic study of methylene blue dye adsorption," *Water Science and Technology*, vol. 84, pp. 1858–1872, 2021, doi: 10.2166/wst.2021.355.

[65] A. N. M. Faizal, A. N. K. Anuar, N. R. Putra, and M. A. A. Zaini, "Methylene blue removal by sodium hydroxide coconut shell-based activated carbons," *Environmental Claims Journal*, vol. 36, pp. 127–140, 2024, doi: 10.1080/10406026.2024.2393604.

[66] S. Krstić et al., "Hydrothermal synthesized and alkaline activated carbons prepared from glucose and fructose: Detailed characterization and testing in heavy metals and methylene blue removal," *Minerals*, vol. 8, Jun. 2018, Art. no. 246, doi: 10.3390/min8060246.

[67] T. O. Ozcelik, E. Altintig, M. Cetinkaya, D. B. Ak, B. Sarici, and A. Ates, "Methylene blue removal using activated carbon from olive pits: Response surface approach and artificial neural network," *Processes*, vol. 13, Jan. 2023, Art. no. 347, doi: 10.3390/pr13020347.